

Tracking a Maneuvering Target Using Two Heterogeneous Passive Sensors on a Single Stationary Platform with IMM Estimation

HONG AN JACK HUANG
YAAKOV BAR-SHALOM
RONG YANG
GEE WAH NG

Bearing-only passive sensors have the advantage of being non-detectable, but they come with target state observability limitations. A new approach, the unscented Gauss-Helmert filter that fuses out-of-sequence acoustic measurements (OOSM-A) and electro-optic (EO) measurements (OOSM-AE), has been developed recently to fuse non-delayed and delayed measurements from two heterogeneous passive sensors on a single platform to overcome these observability issues. In this paper, we extend the OOSM-AE approach to use interacting multiple models (IMM) to improve target tracking accuracy when tracking maneuvering targets. The maneuvers considered are circular motion and S-turns. The resulting IMMOOSM-AE handles the delayed acoustic measurements as out-of-sequence measurements. Scenarios are simulated and tested with both IMMOOSM-AE and OOSM-AE and results are presented.

Manuscript received July 25, 2016; revised November 4, 2016; released for publication December 15, 2016.

Refereeing of this contribution was handled by Paolo Braca.

Authors' addresses: H. A. J. Huang, R. Yang and G. W. Ng, DSO National Laboratories, 12 Science Park Drive, Singapore 118225 (E-mail: hhongan@dso.org.sg; yrong@dso.org.sg; ngeewah@dso.org.sg). Y. Bar-Shalom, Department of ECE, University of Connecticut, Storrs, CT 06269, USA (E-mail: ybs@enr.uconn.edu).

Supported by ARO Grant W911NF-10-1-0369.

1557-6418/17/\$17.00 © 2017 JAIF

I. INTRODUCTION

There are operational merits to using passive sensors. Passive sensors are usually covert and non-detectable. However, range information is usually not available from these sensors. It then becomes challenging to initiate and track a target from a single passive sensor. This is known as the bearing-only tracking (BOT) or target motion analysis (TMA) which has been well studied in the literature [1] [7] [11]. On a single platform, the rate of change of the measurement must not be too small for the target to be observable. In addition, the platform must be able to outmaneuver the target. This means that the sensor platform must be moving with at least one degree of motion greater than the target [8]. For example, if the target is stationary, the sensor platform must be moving. If the target is moving at constant velocity, the sensor platform must be accelerating or performing a turn. It has been shown recently that a passive sensor can estimate the state of a target doing a coordinated turn without observer maneuver under a set of assumptions [9].

It is also possible to use a multiple passive sensor configuration to triangulate targets to provide better position estimates. The shortcoming to this approach is that it requires the sensors to communicate with each other (or to a fusion center) over a large baseline for good position estimation. It is costly to deploy such a sensor configuration over a large area without using radio communication. And if radio is used for communication, then the covert advantage can be lost. Therefore, there is great advantage to have passive sensors co-located on a single stationary platform and yet be able to initiate and track maneuvering targets.

The problem of target tracking in the presence of propagation delay has been studied recently. A number of approaches have been proposed, such as using a particle filter with a successive approximation approach (SAA) [13] [14] and the Unscented Gauss-Helmert Filter (UGHF) [18]. These approaches exploit the propagation delay to provide better estimates of the target state, and have better performance than a naive filter that ignores this phenomenon. The UGHF has been extended to use an interacting multiple model (IMM) estimator [6] [12] to track maneuvering targets [19]. However, these approaches still suffer from the same constraints as traditional BOT problems, i.e. the sensor platform must outmaneuver the target and the rate of change of measurement must not be too small.

A new approach, OOSM-AE, has been proposed in [17] to fuse measurements from two heterogeneous passive sensors on a single platform, one with negligible delay (such as EO or ESM sensor) and one with finite propagation delay (such as an acoustic sensor). The OOSM-AE handles the acoustic measurements as out-of-sequence measurements (OOSM) [2] [3] as they will arrive later than the EO measurements. The OOSM-AE has been demonstrated to improve observability and

TABLE I
List of Acronyms

Acronyms	Definition
AE	Acoustic and EO/ESM fusion
BOT	Bearing-only tracking
CT-H	Coordinated turn model with high process noise
CT-L	Coordinated turn model with low process noise
CV-L	Constant velocity model with low process noise
EO	Electro-optical (sensor)
ESM	Electronic support measures
IMM	Interacting multiple model (estimation)
IMMOOSM-AE	Extension of OOSM-AE that uses IMM
OOSM	Out-of-sequence measurement
OOSM-AE	OOSM algorithm which fuses acoustic and EO measurements
SAA	Successive approximation algorithm
TMA	Target motion analysis
UGHF	Unscented Gauss-Helmert filter

allows the sensor platform to be stationary as long as there is a sufficient rate of change in the measurements. This work enables greater operational flexibility as the platform no longer needs to be outmaneuvering the target in order to initiate and track the target. The main contribution of this paper is how to account properly for the time delay in one of the sensors and take advantage of this delay when tracking a maneuvering target using two sensors on a single non-maneuvering platform.

The aim of this paper is to extend the OOSM-AE fusion approach by combining it with interacting multiple model (IMM) estimation. The IMMOOSM-AE estimator captures target maneuvers by using additional motion models by calculating their likelihoods. Three motion models are used in the present work in IMMOOSM-AE: a low process noise nearly constant velocity model (CV-L), a high process noise coordinated turn model (CT-H) and a low process noise nearly coordinated turn model (CT-L).

Table I presents the lists of acronyms used in this paper.

Section II formulates the problem and defines the target state, measurement models and transition models. In Section III, the track initiation algorithm, which provides a starting track state and covariance for the filter, is described. In Section IV, the tracking filter is presented and the individual steps, such as IMM mixing, model based prediction, retrodiction and update, are described. In Section V, the two test scenarios (circular motion and connected S-turns) are presented and the results for IMMOOSM-AE and OOSM-AE (with three different levels of process noise) are provided. In Section VI, the conclusions are presented.

II. PROBLEM FORMULATION

Both the EO passive sensor, s_1 , and the acoustic passive sensor, s_2 , are assumed to be co-located on a stationary platform at $\mathbf{x}^s = [x^s, y^s]'$. For simplicity, $\dot{x}^s = \dot{y}^s = 0$ in this paper.

The target state for the EO sensor is

$$\mathbf{x}^E(t_k^{s_1}) = [x(t_k^{s_1}) \quad y(t_k^{s_1}) \quad \dot{x}(t_k^{s_1}) \quad \dot{y}(t_k^{s_1}) \quad \omega(t_k^{s_1})]'$$
 (1)

where $t_k^{s_1}$ is time at which the k^{th} EO signal is received by the EO sensor; x , y , \dot{x} , \dot{y} denote the position and velocity of the target and ω denotes the turn rate. We assume that the delay in propagation for EO signal is negligible, i.e. $t_k^{s_1} = t_k^{e_1}$, where $t_k^{e_1}$ is the time at which the signal is emitted from the target.

The measurement model for the EO sensor is¹

$$\mathbf{z}(t_k^{s_1}) = \tan^{-1} \left[\frac{x(t_k^{s_1}) - x^s}{y(t_k^{s_1}) - y^s} \right] + w_{s_1}(t_k^{s_1})$$
 (2)

where w_{s_1} is the zero mean white Gaussian measurement noise, with variance $\sigma_{s_1}^2$.

The transition model for the EO sensor is

$$\mathbf{x}^E(t_k^{s_1}) = f^*[\mathbf{x}^E(t_{k-1}^{s_1}, t_k^{s_1}, t_{k-1}^{s_1})] + v^*(t_k^{s_1}, t_{k-1}^{s_1})$$
 (3)

where $f(\cdot)$ is the transition function, v is the process noise, and $*$ stands for the different motion models given later in (30) and (33).

The acoustic sensor detects the target with a propagation delay. The target state for the acoustic sensor is

$$\mathbf{x}^A(t_j^{e_2}) = [x(t_j^{e_2}) \quad y(t_j^{e_2}) \quad \dot{x}(t_j^{e_2}) \quad \dot{y}(t_j^{e_2}) \quad \omega(t_j^{e_2}) \quad t_j^{e_2}]'$$
 (4)

where $t_j^{e_2}$ is time at which the j^{th} acoustic signal is emitted by the target. Note that the acoustic target state includes the emission time $t_j^{e_2}$.

The time delay the acoustic sensor detects the target state with is denoted by $\delta_{j,\ell}$. The relationship between the target acoustic emission time $t_j^{e_2}$ and the sensor receive time $t_\ell^{s_2}$ is

$$t_j^{e_2} = t_\ell^{s_2} - \delta_{j,\ell}$$
 (5)

where the delay is given by

$$\delta_{j,\ell} = \frac{r_{j,\ell}}{c^p}$$
 (6)

with $r_{j,\ell}$ the range from the target at $t_j^{e_2}$ to the sensor² at $t_\ell^{s_2}$, and c^p is the propagation speed of sound in the medium (air or water).

The measurement model for the acoustic sensor is

$$\mathbf{z}(t_j^{s_2}) = \tan^{-1} \left[\frac{x(t_j^{e_2}) - x^s}{y(t_j^{e_2}) - y^s} \right] + w_{s_2}(t_j^{e_2})$$
 (7)

where w_{s_2} is a zero-mean white Gaussian measurement noise with variance $\sigma_{s_2}^2$.

An illustration of the emission and reception times is given in Fig. 1.

Due to the propagation delay described in (5), the state transition model is implicit (see (8)) and a Gauss-Helmert model is required to represent the implicit state transition. The Gauss-Helmert model has been shown to be equivalent to the Markov model used in a Kalman

¹The present work assumes perfect data association.

²The sensor can move, but we considered a stationary sensor since this is the most difficult situation for passive tracking.

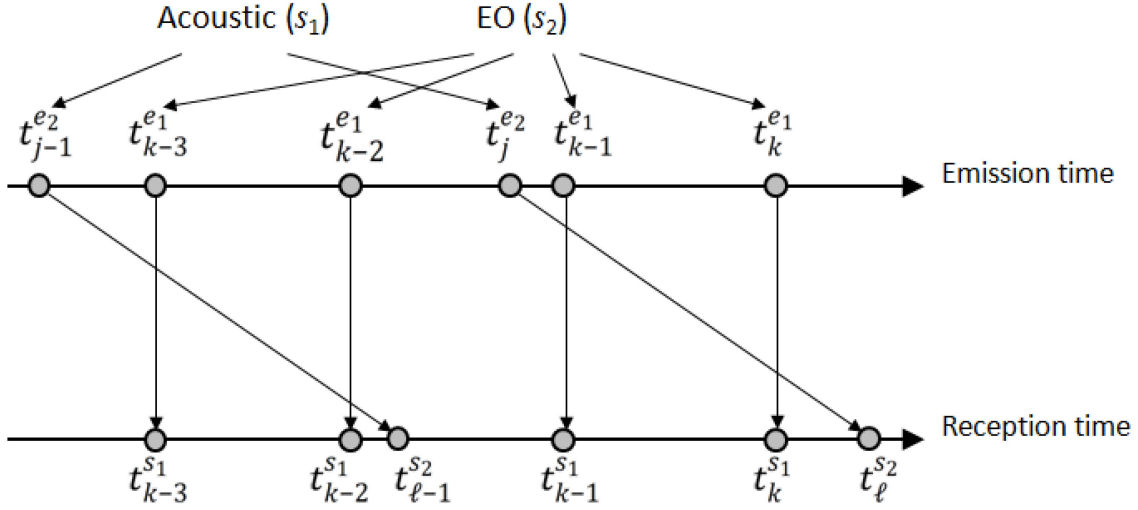


Fig. 1. Illustration of emission time and reception time

filter in [16]. However, there is no explicit formula obtainable for a retrodicted (or predicted) state from a current state. The Gauss-Helmert transition model is used for performing retrodiction and state update with the OOSM in Section IV-B.1 and the transition model is, instead of (3), of the following implicit form

$$g^*[\mathbf{x}^A(t_j^{e2}), \mathbf{x}^E(t_k^{s1})] + v^*(t_j^{e2}, t_k^{s1}) = \mathbf{0}_6 \quad (8)$$

where $\mathbf{x}^E(t_k^{s1})$ is the latest track state, $\mathbf{x}^A(t_j^{e2})$ is the state at the time at which the acoustic signal is emitted, $g(\cdot)$ is the Gauss-Helmert transition function, v is the process noise, $\mathbf{0}_6$ is the 6-dimensional zero vector and $*$ stands for the different motion models used in the IMMOOSM-AE given later in (55) and (69). Note that the \mathbf{x}^E state has dimension 5 while the \mathbf{x}^A state has dimension 6. The track is maintained in the 5-dimensional \mathbf{x}^E state while the 6-dimensional \mathbf{x}^A state is only used during retrodiction and OOSM innovation calculation using UGHF.

III. TRACK INITIATION

Given an initial batch of EO and acoustic bearing-only measurements from a single stationary platform,

$$\mathbf{z} = [z(t_1^s) \dots z(t_n^s)]' \quad s \in \{s_1, s_2\} \quad (9)$$

we want to initiate a track at time t_n^s . We define the initial track state, \mathbf{x} , at time t_n^s (the end of the initialization batch)

$$\mathbf{x} = [x(t_n^s) \quad y(t_n^s) \quad \dot{x}(t_n^s) \quad \dot{y}(t_n^s)]' \quad (10)$$

We assume that the target is moving at a constant velocity during the initialization batch.³ The relationship between \mathbf{x} and \mathbf{z} is

$$\mathbf{z} = \mathbf{h}(\mathbf{x}) + \mathbf{w} \quad (11)$$

³Other motion models can be used.

where component k of \mathbf{h} is

$$\mathbf{h}_k(\mathbf{x}, t_k^s) = \begin{cases} \tan^{-1} \left[\frac{x + \dot{x}(t_k^s - t_n^s) - x^s}{y + \dot{y}(t_k^s - t_n^s) - y^s} \right] & \text{if } s = s_1 \\ \tan^{-1} \left[\frac{x + \dot{x}(t_k^s - t_n^s - \delta_{j,k}) - x^s}{y + \dot{y}(t_k^s - t_n^s - \delta_{j,k}) - y^s} \right] & \text{if } s = s_2 \end{cases} \quad (12)$$

where $\delta_{j,k}$ is the time delay (6) for the acoustic signals and \mathbf{w} is the batch measurement noise.

We assume \mathbf{w} is zero mean Gaussian, with uncorrelated components. The covariance of \mathbf{w} (assuming for simplicity that $\sigma_{s_1} = \sigma_{s_2} = \sigma_b$) is

$$\mathbf{R} = \sigma_b^2 \mathbf{I}_n \quad (13)$$

where \mathbf{I}_n is the $n \times n$ identity matrix.

The estimate of the state \mathbf{x} can be obtained using the maximum likelihood (ML) approach by solving the following nonlinear least squares problem [4]

$$\hat{\mathbf{x}} = \arg \min_{\mathbf{x}} \{[\mathbf{z} - \mathbf{h}(\mathbf{x})]' \mathbf{R}^{-1} [\mathbf{z} - \mathbf{h}(\mathbf{x})]\} \quad (14)$$

The Jacobian matrix of $\mathbf{h}(\cdot)$, required for solving the above,

$$\mathbf{H}(\mathbf{x}) = (\nabla_{\mathbf{x}} \mathbf{h}[\mathbf{x}]') \quad (15)$$

can be obtained by performing numerical partial differentiation on $\mathbf{h}(\cdot)$ with respect to each component of \mathbf{x} as in [17].

The track initiation algorithm is described in Table II where ℓ_{\max} is the maximum number of iterations before it terminates and $\mathbf{d}_{\text{threshold}}$ is the threshold value for the step size below which it terminates.

IV. THE TRACKING FILTER

The inputs to the dynamic state estimator are the EO and acoustic measurements. The EO measurements arrive instantaneously, while the acoustic measurements arrive with a propagation delay. The estimator updates the state at the EO measurement times and treats the acoustic measurements as out-of-sequence measure-

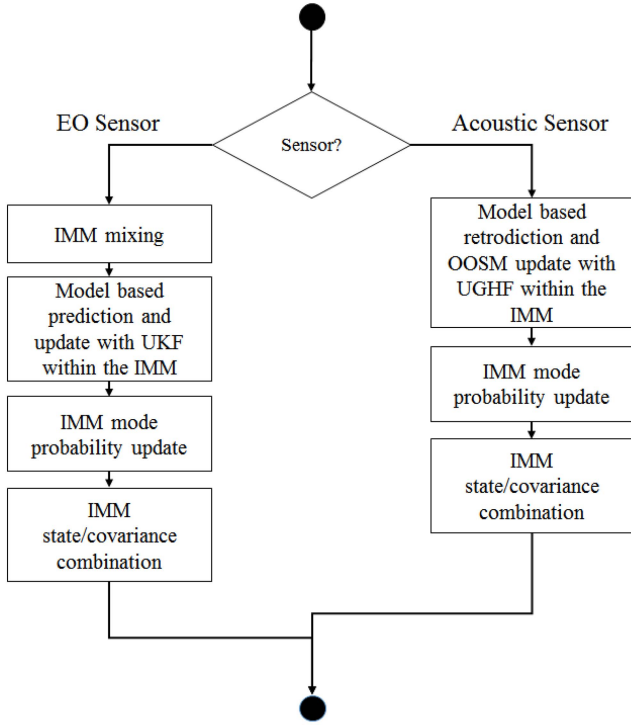


Fig. 2. Overview of IMMOOSM-AE estimator

$$\Pi(T) = \frac{1}{\lambda} \begin{bmatrix} \lambda_2 + \lambda_3 + \lambda_1 e^{-\lambda T} & \alpha[\lambda_1 - \lambda_1 e^{-\lambda T}] & (1 - \alpha)[\lambda_1 - \lambda_1 e^{-\lambda T}] \\ \beta[\lambda_2 - \lambda_2 e^{-\lambda T}] & \lambda_1 + \lambda_3 + \lambda_2 e^{-\lambda T} & (1 - \beta)[\lambda_2 - \lambda_2 e^{-\lambda T}] \\ \gamma[\lambda_3 - \lambda_3 e^{-\lambda T}] & (1 - \gamma)[\lambda_3 - \lambda_3 e^{-\lambda T}] & \lambda_1 + \lambda_2 + \lambda_3 e^{-\lambda T} \end{bmatrix} \quad (19)$$

ments (OOSM). An overview of a single cycle of the estimator is shown in Fig. 2.

The IMM incorporates 3 motion models: CV-L (nearly constant velocity, with low process noise—white noise acceleration), CT-H and CT-L (nearly coordinated turn with high and low noise). Model 1 is CV-L, model 2 is CT-H and model 3 is CT-L. The purpose of the CV-L is to capture the constant velocity motion. Likewise, the purpose of the CT-L is to capture the ongoing coordinated turn maneuvers. The purpose of the CT-H model is to facilitate the abrupt change from CV-L to CT-L and vice versa (turn onset and termination). The turn rate, ω , must be allowed to switch from zero (during constant velocity) to a non-zero value (during coordinated turn) in a short time. Using only CV-L and CT-L with low process noise in the turn rate will not enable the estimator to follow this change quickly.

A. EO Measurements

This section describes how the EO measurements are handled in the IMM estimator.

1) IMM Mixing:

In IMM estimation, a mode probability, μ_k^i , is calculated for each motion model i at time k . The IMM

TABLE II
Track Initiation

- 1) Compute initial estimate $\hat{\mathbf{x}}^0$ based on EO bearing measurement at t_n^s and a moderate range and zero velocity.
- 2) Initialize $\ell = 0$.
- 3) While $\ell < \ell_{\max}$ or $|\mathbf{d}| > \mathbf{d}_{\text{threshold}}$
 - a) $\mathbf{P}^\ell = [\mathbf{H}(\hat{\mathbf{x}}^\ell)'\mathbf{R}^{-1}\mathbf{H}(\hat{\mathbf{x}}^\ell)]^{-1}$ (16)
 - b) $\mathbf{d} = \mathbf{P}^\ell[\mathbf{H}(\hat{\mathbf{x}}^\ell)'\mathbf{R}^{-1}[\mathbf{z} - \mathbf{h}(\hat{\mathbf{x}}^\ell)]]$ (17)
 - c) $\hat{\mathbf{x}}^{\ell+1} = \hat{\mathbf{x}}^\ell + \mathbf{d}$ (18)
- 4) Assign $\hat{\mathbf{x}}^\ell$ and \mathbf{P}^ℓ as the initiated track state and covariance.

estimation is able to capture the motion model change by dynamically adjusting μ^i according to the filter update. For example, a target can move with nearly constant velocity and subsequently perform a coordinated turn. Then, μ^1 for CV-L model will become the highest among the different motion models during its constant velocity motion at the start and, subsequently, μ^3 for the CT-L model will become highest during the turning motion. The evolution of the mode probabilities, μ^i , depends on the transition probability matrix Π .

The transition probability matrix, Π , used in the present work is a generalization of the discretized continuous-time Markov chain transition probability matrix from Eq. (2.6.6-15) in [5].

where, with λ_m , $m = 1, 2, 3$, the transition probability rates (their inverses are the expected sojourn times in the corresponding states of the Markov chain),

$$\lambda = \sum_{n=1}^3 \lambda_n \quad (20)$$

$$T = |t_k^{s_1} - t_{k-1}^{s_1}| \quad (21)$$

for EO IMM mixing (the prediction time interval) or

$$T = |t_j^{e_2} - t_k^{s_1}| \quad (22)$$

for acoustic OOSM mode probability update,⁴ and α , β and γ are normalizing factors which are introduced to keep the sum of the row elements of Π to be unity.⁵

⁴This is the difference between the time stamp of the acoustic measurement and the time for which the state update is performed (the retrodiction interval, see (39) in the sequel). See Fig. 1 for the time notations.

⁵The 2-dimensional Markov chain transition matrix is rigorously derived in Papoulis [15] from the continuous-time chain with appropriate transition rates. The 3-dimensional continuous-time Markov chain does not have an explicit transition matrix, so this is the generalization of the 2-dimensional Markov chain transition matrix to 3 dimensions by adding another transition rate.

In IMMOOSM-AE, Π is a 3×3 matrix, since three motion models are used: CV-L, CT-H, and CT-L. The CV model assumes the turn rate to be zero while the two CT models include the turn rate. Thus, unbiased mixing must be done [20]. The weighted sum of the probabilities corresponding to turning (μ^2, μ^3) from the two CT models are transferred to the modified state and covariance for the CV model for the purpose of mixing. This ensures that the resulting elements corresponding to turn rate ($\hat{\omega}^2, \hat{\omega}^3$) in the two CT models are unbiased after mixing. The modification is done according to [20] as follows:

$$\hat{\mathbf{x}}_M^{\text{E1}} = \begin{bmatrix} \hat{\mathbf{x}}_c^{\text{E1}} \\ \hat{\omega}^2 \mu_{2|1} + \hat{\omega}^3 \mu_{3|1} \end{bmatrix} \quad (23)$$

$$\mathbf{P}_M^{\text{E1}} = \begin{bmatrix} \mathbf{P}_c^{\text{E1}} & 0 \\ 0 & \mathbf{P}_\omega^{\text{E2}} \mu_{2|1} + \mathbf{P}_\omega^{\text{E3}} \mu_{3|1} \end{bmatrix} \quad (24)$$

where $\hat{\mathbf{x}}_c^{\text{E1}}$ and \mathbf{P}_c^{E1} are the blocks common to both CV and CT models, i.e. corresponding to the x , y , \dot{x} and \dot{y} states and $\mu_{2|1}$, $\mu_{3|1}$ are the IMM mixing probabilities [4].

TABLE III
IMM Mixing

$$\mu^i(t_k^{s_1} | t_{k-1}^{s_1}) = \sum_{n=1}^m \Pi_{ni} \mu^n(t_{k-1}^{s_1}) \quad (25)$$

$$\mu^{n|i}(t_{k-1}^{s_1}) = \frac{\Pi_{ni} \mu^n(t_{k-1}^{s_1})}{\mu^i(t_k^{s_1} | t_{k-1}^{s_1})} \quad (26)$$

$$\hat{\mathbf{x}}^{\text{E0}i}(t_{k-1}^{s_1}) = \sum_{n=1}^m \hat{\mathbf{x}}^{\text{E}n}(t_{k-1}^{s_1}) \mu^{n|i}(t_{k-1}^{s_1}) \quad (27)$$

$$\mathbf{P}^{\text{E0}i}(t_{k-1}^{s_1}) = \sum_{n=1}^m \mu^{n|i}(t_{k-1}^{s_1}) [\mathbf{P}^{\text{E}n}(t_{k-1}^{s_1}) + (\hat{\mathbf{x}}^{\text{E}n}(t_{k-1}^{s_1}) - \hat{\mathbf{x}}^{\text{E0}i}(t_{k-1}^{s_1})) (\hat{\mathbf{x}}^{\text{E}n}(t_{k-1}^{s_1}) - \hat{\mathbf{x}}^{\text{E0}i}(t_{k-1}^{s_1}))'] \quad (28)$$

$$(\hat{\mathbf{x}}^{\text{E}n}(t_{k-1}^{s_1}) - \hat{\mathbf{x}}^{\text{E0}i}(t_{k-1}^{s_1}))'] \quad (29)$$

The IMM mixing uses the mixing probability (26) based on the transition probability matrix, Π , and com-

putes the initial estimate $\hat{\mathbf{x}}_{k-1}^{\text{E0}i}$ and covariance $\mathbf{P}_{k-1}^{\text{E0}i}$ according to (27) and (28), respectively, where i corresponds to each model. The IMM mixing steps are given in Table. III, and the mixed estimates and covariances from t_{k-1} are used as initial condition for the mode-matched filters at time t_k in Section IV-A.2.

2) Prediction and Update using UKF:

The unscented Kalman filter (UKF) is used to predict and update the state for each mode with the EO measurements.

The transition model, f^{CV} , and process noise, \mathbf{Q}^{CV} , for the CV model⁶ are given below.

$$f^{\text{CV}}[\mathbf{x}^{\text{E}}(t_{k-1}^{s_1}), T_{k,k-1}] = \begin{bmatrix} 1 & 0 & T_{k,k-1} & 0 & 0 \\ 0 & 1 & 0 & T_{k,k-1} & 0 \\ 0 & 0 & 1 & 0 & 0 \\ 0 & 0 & 0 & 1 & 0 \\ 0 & 0 & 0 & 0 & 0 \end{bmatrix} \mathbf{x}^{\text{E}}(t_{k-1}^{s_1}) \quad (30)$$

$$E[v^{\text{CV}}(\cdot)v^{\text{CV}}(\cdot)'] = \mathbf{Q}^{\text{CV}}(t_k^{s_1} - t_{k-1}^{s_1}) = \begin{bmatrix} \frac{T_{k,k-1}^3}{3} & 0 & \frac{T_{k,k-1}^2}{2} & 0 & 0 \\ 0 & \frac{T_{k,k-1}^3}{3} & 0 & \frac{T_{k,k-1}^2}{2} & 0 \\ \frac{T_{k,k-1}^2}{2} & 0 & T_{k,k-1} & 0 & 0 \\ 0 & \frac{T_{k,k-1}^2}{2} & 0 & T_{k,k-1} & 0 \\ 0 & 0 & 0 & 0 & 0 \end{bmatrix} q \quad (31)$$

where

$$T_{k,k-1} = t_k^{s_1} - t_{k-1}^{s_1} \quad (32)$$

where q is the process noise power spectral density (PSD) that affects the x , y , \dot{x} and \dot{y} states. The physical dimension of q is acceleration²/frequency.

The transition model, f^{CT} , and process noise, \mathbf{Q}^{CT} , for the CT model are given below.

$$f^{\text{CT}}[\mathbf{x}^{\text{E}}(t_{k-1}^{s_1}), T_{k,k-1}] = \begin{bmatrix} 1 & 0 & \frac{\sin[\omega(t_{k-1}^{s_1})T_{k,k-1}]}{\omega(t_{k-1}^{s_1})} & -\frac{1 - \cos[\omega(t_{k-1}^{s_1})T_{k,k-1}]}{\omega(t_{k-1}^{s_1})} & 0 \\ 0 & 1 & \frac{1 - \cos[\omega(t_{k-1}^{s_1})T_{k,k-1}]}{\omega(t_{k-1}^{s_1})} & \frac{\sin[\omega(t_{k-1}^{s_1})T_{k,k-1}]}{\omega(t_{k-1}^{s_1})} & 0 \\ 0 & 0 & \cos[\omega(t_{k-1}^{s_1})T_{k,k-1}] & -\sin[\omega(t_{k-1}^{s_1})T_{k,k-1}] & 0 \\ 0 & 0 & \sin[\omega(t_{k-1}^{s_1})T_{k,k-1}] & \cos[\omega(t_{k-1}^{s_1})T_{k,k-1}] & 0 \\ 0 & 0 & 0 & 0 & 1 \end{bmatrix} \mathbf{x}^{\text{E}}(t_{k-1}^{s_1}) \quad (33)$$

⁶This is actually a white noise acceleration (WNA) model.

TABLE IV
The UKF steps

- 1) Generate the preliminary sigma points and weights based on the initial estimate $\hat{\mathbf{x}}^{E0i}(t_{k-1}^{s1})$ and covariance $\mathbf{P}^{E0i}(t_{k-1}^{s1})$ [10]; i denotes the mode.
- 2) Predict the preliminary sigma points using transition model, f .
- 3) Compute predicted $\hat{\mathbf{x}}^{Ei}(t_k^{s1} | t_{k-1}^{s1})$ and $\mathbf{P}^{Ei}(t_k^{s1} | t_{k-1}^{s1})$ based on propagated sigma points and weights.
- 4) Add the model process noise \mathbf{Q}^* to $\mathbf{P}^{Ei}(t_k^{s1} | t_{k-1}^{s1})$ where \mathbf{Q}^{CV} and \mathbf{Q}^{CT} are given in (31) and (34).
- 5) Recalculate the sigma points to account for the added process noise covariance.
- 6) Compute the predicted $\hat{\mathbf{z}}^i(t_k^{s1} | t_{k-1}^{s1})$ based on the propagated sigma points and weight using the measurement model.
- 7) Calculate the innovation covariance $S^{Ei}(t_k^{s1})$.
- 8) Use the sensor measurement $\mathbf{z}(t_k^{s1})$ to obtain the innovation $\nu^{Ei}(t_k^{s1})$, the updated state $\hat{\mathbf{x}}^{Ei}(t_k^{s1})$, and covariance $\mathbf{P}^{Ei}(t_k^{s1})$.

$$\begin{aligned}
& E[\nu^{CT}(\cdot)\nu^{CT}(\cdot)'] \\
&= \mathbf{Q}^{CT}(t_k^{s1} - t_{k-1}^{s1}) \\
&= \mathbf{Q}^{CV}(t_k^{s1} - t_{k-1}^{s1}) + \begin{bmatrix} 0 & 0 & 0 & 0 & 0 \\ 0 & 0 & 0 & 0 & 0 \\ 0 & 0 & 0 & 0 & 0 \\ 0 & 0 & 0 & 0 & 0 \\ 0 & 0 & 0 & 0 & T_{k,k-1} \end{bmatrix} q_\omega
\end{aligned} \tag{34}$$

where

$$T_{k,k-1} = t_k^{s1} - t_{k-1}^{s1} \tag{35}$$

where q_ω is the process noise PSD that affects the ω state (angular rate). The physical dimension of q_ω is (angular acceleration)²/frequency

The UKF prediction and update are performed for each model as described in Table IV.

- 3) Mode Probability Update and State Estimate/
Covariance Combination:

With the mode-conditioned innovation, $\nu^{Ei}(t_k^{s1})$, and its covariance, $S^{Ei}(t_k^{s1})$, the mode probabilities, $\mu^i(t_k^{s1})$, are updated as

$$\mu^i(t_k^{s1}) = \frac{\mu^i(t_k^{s1} | t_{k-1}^{s1}) \mathcal{N}(\nu^{Ei}(t_k^{s1}); 0, S^{Ei}(t_k^{s1}))}{\sum_{n=1}^m \mu^n(t_k^{s1} | t_{k-1}^{s1}) \mathcal{N}(\nu^{En}(t_k^{s1}); 0, S^{En}(t_k^{s1}))} \tag{36}$$

where $\mathcal{N}(\nu^{Ei}(t_k^{s1}); 0, S^{Ei}(t_k^{s1}))$ is the model likelihood function based on the latest measurement.

The combined state estimate, $\hat{\mathbf{x}}^E(t_k^{s1})$, and covariance, $\mathbf{P}^E(t_k^{s1})$, are obtained as

$$\hat{\mathbf{x}}^E(t_k^{s1}) = \sum_{n=1}^m \mu^n(t_k^{s1}) \hat{\mathbf{x}}^{En}(t_k^{s1}) \tag{37}$$

$$\begin{aligned}
\mathbf{P}^E(t_k^{s1}) &= \sum_{n=1}^m \mu^n(t_k^{s1}) [\mathbf{P}^{En}(t_k^{s1}) \\
&+ (\hat{\mathbf{x}}^{En}(t_k^{s1}) - \hat{\mathbf{x}}^E(t_k^{s1})) (\hat{\mathbf{x}}^{En}(t_k^{s1}) - \hat{\mathbf{x}}^E(t_k^{s1}))']
\end{aligned} \tag{38}$$

B. Acoustic Measurements

This section describes how the acoustic measurements are handled in the IMM estimator. Acoustic measurements arrive later than the EO measurement due to the slower propagation of sound, i.e. they are OOSM and they are incorporated into the IMM according to the procedure described in Sec. 2.6.6 of [5]. The current state estimate must be retrodicted back in time to the time of acoustic signal emission before the update. This is handled by the Unscented Gauss-Helmert Filter (UGHF) retrodiction and the update with the OOSM is then carried out as described in the sequel.

- 1) Retrodiction and OOSM innovation calculation using UGHF:

The process noise is not taken into consideration in the state for algorithm C⁷ (see Sec 2.6.3 of [5]).⁸ The Gauss-Helmert model (GHM) is thus replaced by

$$g^*[\hat{\mathbf{x}}^A(t_j^{e2} | t_k^{s1}), \hat{\mathbf{x}}^E(t_k^{s1})] = \mathbf{0}_6 \tag{39}$$

where $\hat{\mathbf{x}}^A(t_j^{e2} | t_k^{s1})$ is the (6-dimensional) retrodicted state, which also includes the emission time, required for the measurement update and $\hat{\mathbf{x}}^E(t_k^{s1})$ is the latest (5-dimensional) track state estimate.

The Markov model used in a Kalman filter relies on an explicit form of the state transition model. In contrast, the GHM is for situations where there is only an implicit transition model and it uses the Gauss-Newton algorithm to obtain the retrodicted state by solving (39). The Gauss-Newton iteration with index p is

$$\begin{aligned}
& [\hat{\mathbf{x}}^A(t_j^{e2} | t_k^{s1})]^p \\
&= [\hat{\mathbf{x}}^A(t_j^{e2} | t_k^{s1})]^{p-1} - \mathbf{A}^{-1} g^* [[\hat{\mathbf{x}}^A(t_j^{e2} | t_k^{s1})]^{p-1}, \hat{\mathbf{x}}^E(t_k^{s1})]
\end{aligned} \tag{40}$$

where \mathbf{A} is the Jacobian matrix

$$\mathbf{A} = \frac{\partial g^* [[\hat{\mathbf{x}}^A(t_j^{e2} | t_k^{s1})]^p, \hat{\mathbf{x}}^E(t_k^{s1})]}{\partial [[\hat{\mathbf{x}}^A(t_j^{e2} | t_k^{s1})]^p]} \tag{41}$$

and $[\cdot]^p$ indicates the estimated value in the p th iteration. The algorithm is terminated when $p = 1000$ or

$$\frac{|[\hat{\mathbf{x}}^A(t_j^{e2} | t_k^{s1})]^p - [\hat{\mathbf{x}}^A(t_j^{e2} | t_k^{s1})]^{p-1}|}{|[\hat{\mathbf{x}}^A(t_j^{e2} | t_k^{s1})]^{p-1}|} < 0.1 \tag{42}$$

The GHM for CV and CT can be found in Appendix A and Appendix B respectively. The starting point for the Gauss-Newton algorithm, $[\hat{\mathbf{x}}^A(t_j^{e2} | t_k^{s1})]^0$, is computed by assuming the initial emission time

$$[t_j^{e2}]^0 = t_k^{s1} - \frac{\sqrt{x(t_k^{s1})^2 + y(t_k^{s1})^2}}{c^p} \tag{43}$$

⁷This is the simplest retrodiction algorithm, which does not take into account the process noise.

⁸This is one of the algorithms presented in [5], chosen for the present work.

TABLE V
Retrodiction and Update with OOSM in UGHF

- 1) Generate sigma points and weights based on $\hat{\mathbf{x}}^{Ei}(t_k^{s1})$ and $\mathbf{P}^{Ei}(t_k^{s1})$; i denotes the mode.
- 2) Retrodicit sigma points with the transition model, g , using the Gauss-Newton algorithm.
- 3) Compute $\hat{\mathbf{x}}^{Ai}(t_j^{e2} | t_k^{s1})$ and $\mathbf{P}^{Ai}(t_j^{e2} | t_k^{s1})$ based on propagated sigma points and weights.
- 4) Compute the retrodicted measurement $\hat{\mathbf{z}}^i(t_j^{e2} | t_k^{s1})$ based on the propagated sigma points and weights using the measurement model.
- 5) Calculate innovation covariance $S^{Ai}(t_k^{s1}, t_j^{e2})$.
- 6) Use the sensor measurement $\mathbf{z}(t_j^{s2})$ to obtain innovation $\nu^{Ai}(t_k^{s1}, t_j^{e2})$, the updated state $\hat{\mathbf{x}}^{Ei}(t_k^{s1}, t_j^{e2})$ and the updated covariance $\mathbf{P}^{Ei}(t_k^{s1}, t_j^{e2})$.

With the initial emission time $[t_j^{e2}]^0$, the remaining elements in the initial $[\hat{\mathbf{x}}^A(t_j^{e2} | t_k^{s1})]^0$ can be computed from $\hat{\mathbf{x}}^E(t_k^{s1})$ using the standard CV and CT transition model, f , given in (30) and (33), respectively.

The UGHF retrodiction and its update with the OOSM are done for each model as described in Table V.

- 2) Mode probability and state update with the OOSM and state/covariance combination:

The mode probability update with the acoustic measurements is described here. The transition probability matrix $\Pi(T)$ from (19), with $T_{j,k} = |t_j^{e2} - t_k^{s1}|$, is used for the mode probability update with the OOSM as

$$\begin{aligned} \mu^i(t_k^{s1}, t_j^{e2}) \\ = \frac{1}{c} \left[\sum_{n=1}^m \mathcal{N}(\nu^{An}(t_k^{s1}, t_j^{e2}); 0, S^{An}(t_k^{s1}, t_j^{e2})) \Pi_{in} \right] \mu^i(t_k^{s1}) \end{aligned} \quad (44)$$

where $\mu^i(t_k^{s1}, t_j^{e2})$ is the updated mode probability at t_k^{s1} using the OOSM from t_j^{e2} .

$$c = \sum_{\ell=1}^m \sum_{n=1}^m \mathcal{N}(\nu^{An}(t_k^{s1}, t_j^{e2}); 0, S^{An}(t_k^{s1}, t_j^{e2})) \Pi_{ln} \mu^\ell(t_k^{s1}) \quad (45)$$

The state and covariance combination is done following the update as follows:

$$\hat{\mathbf{x}}^E(t_k^{s1}, t_j^{e2}) = \sum_{n=1}^m \mu^n(t_k^{s1}, t_j^{e2}) \hat{\mathbf{x}}^{En}(t_k^{s1}, t_j^{e2}) \quad (46)$$

$$\begin{aligned} \mathbf{P}^E(t_k^{s1}, t_j^{e2}) = \sum_{n=1}^m \mu^n(t_k^{s1}, t_j^{e2}) [\mathbf{P}^{En}(t_k^{s1}, t_j^{e2}) \\ + (\hat{\mathbf{x}}^{En}(t_k^{s1}, t_j^{e2}) - \hat{\mathbf{x}}^E(t_k^{s1}, t_j^{e2})) \\ (\hat{\mathbf{x}}^{En}(t_k^{s1}, t_j^{e2}) - \hat{\mathbf{x}}^E(t_k^{s1}, t_j^{e2}))'] \end{aligned} \quad (47)$$

V. SCENARIOS AND RESULTS

Two scenarios are generated and tested by IMMOOSM-AE and OOSM-AE. Three variants of OOSM-AE with different levels of process noise are

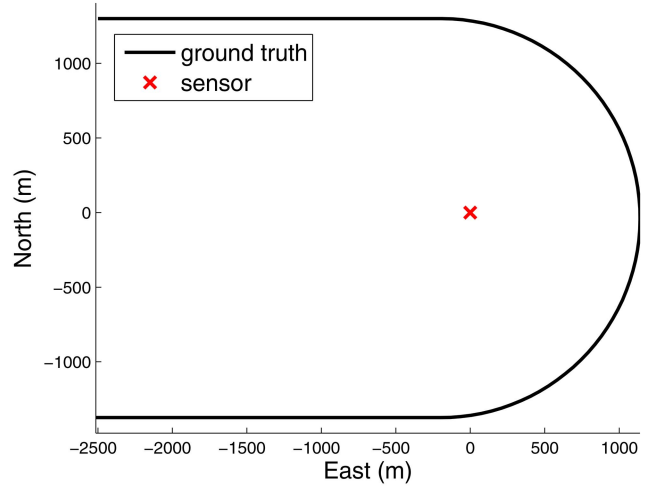


Fig. 3. U-turn scenario

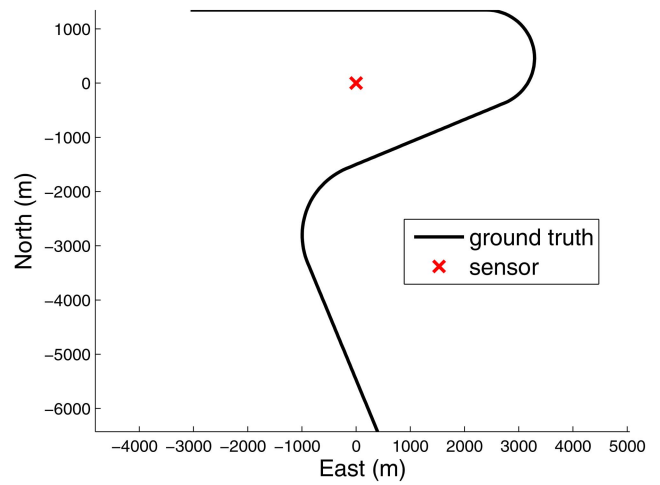


Fig. 4. S-turn scenario

tested. In the U-turn scenario, the target starts at $(-2500, 1300)$ and travels east at 70 m/s for 35 s. Then, it makes a right 3 deg/s turn for 60 s (acceleration of 3.7 m/s²). Finally, it travels west at 70 m/s for 35 s. An illustration is given in Fig. 3. In the S-turn scenario, the target starts at $(-3000, 1350)$ and travels east at 70 m/s for 80 s. Next, it makes a right 4.5 deg/s turn for 35 s (acceleration of 5.5 m/s²). Next, it travels west-southwest at 70 m/s for 45 s. Next, it makes a left 3 deg/s turn for 30 s (acceleration of 3.7 m/s²). Finally, it travels south-south-east at 70 m/s for 50 s. This is illustrated in Fig. 4.

For OOSM-AE which consists of a single CV model using Eq. (1.5.2-5) from [5], the process noise PSD for the single-model (compromise) filter is chosen as

$$q = a_{ave}^2 \tau \quad (48)$$

with $a_{ave} = 1.4 \text{ m/s}^2$ (compromise between exact CV motion and turn which has $a = 3.5 \text{ m/s}^2$) and $\tau = 1 \text{ s}$, one obtains $q = 2 \text{ m}^2/\text{s}^3$; τ is defined as the time interval

over which the acceleration is assumed to be approximately constant. The scenarios are tested by three variants of OOSM-AE: OOSM-AE-Q1 with $q_1 = 2 \text{ m}^2/\text{s}^3$, OOSM-AE-Q2 with $q_2 = 4 \text{ m}^2/\text{s}^3$ (which corresponds to $a = 2 \text{ m/s}^2$) and OOSM-AE-Q3 with $q_3 = 9 \text{ m}^2/\text{s}^3$ (which corresponds to $a = 3 \text{ m/s}^2$).

IMMOOSM-AE consists of 3 models: CV-L, CT-H and CT-L. For the CT-H and the CT-L model, the process noise PSD is obtained using the formula (1.5.3-5) from [5] (modified for turn rate increments)

$$q_\omega = \left(\frac{\Delta\omega}{\tau} \right)^2 \tau = \frac{(\Delta\omega)^2}{\tau} \quad (49)$$

With $\Delta\omega = 1 \text{ deg/s}$ and $\tau = 1 \text{ s}$, one obtains $q_\omega^H = 1 \text{ deg}^2/\text{s}^3$ for the CT-H model. With $\Delta\omega = 0.1 \text{ deg/s}$ and $\tau = 1 \text{ s}$, one has $q_\omega^L = 0.01 \text{ deg}^2/\text{s}^3$ for the CT-L model. For the CV-L model, the process noise PSD is chosen using acceleration $a = \Delta\omega v$ where $v = 70 \text{ m/s}$ and $\Delta\omega = 0.1 \text{ deg/s}$. This yields

$$a = \Delta\omega v = 0.1 \text{ deg/s} \cdot 70 \text{ m/s} = \frac{0.1\pi}{180} \cdot 70 = 0.12 \text{ m/s}^2 \quad (50)$$

Using (48) and (50), the PSD for CV-L is taken as $q = 1.5 \cdot 10^{-2} \text{ m}^2/\text{s}^3$.

The exponential sojourn time distribution parameter for the computing the transition probability are set to be $\lambda_1 = \lambda_3 = 10^{-2} \text{ s}^{-1}$ and $\lambda_2 = 0.2 \text{ s}^{-1}$. The normalizing factors for the transition probability matrix (19) are set as follows: $\alpha = 0.9$, $\beta = 0.5$ and $\gamma = 0.1$.

For both of the scenarios, the sensor is stationary at the origin. Both the EO and acoustic sensor have measurement error with $\sigma_b = 1 \text{ deg}$. The sampling period for the EO sensor is 1 s, while the sampling period for the acoustic sensor is 2 s. The propagation speed of sound, c^p , is 344 m/s.

The first 20 s of measurements data are used for track initiation assuming exact CV motion. Subsequently, OOSM-AE-Q1, OOSM-AE-Q2, OOSM-AE-Q3 and IMMOOSM-AE are used to track the target.

100 Monte Carlo runs are generated and the average root-mean-square error (RMSE) for position and velocity are presented in Tables VI and VII. The average position $\overline{\text{RMSE}}_k^p(N)$ at time k from N Monte Carlo runs, is calculated as follows

$$\overline{\text{RMSE}}_k^p(N) = \sqrt{\frac{1}{N} \sum_{n=1}^N \|\hat{\mathbf{x}}_k^p(n) - \mathbf{x}_k^{\text{pg}}\|^2} \quad (51)$$

where $\hat{\mathbf{x}}_k^p(n)$ is the position state estimate at time k for run n , \mathbf{x}_k^{pg} is the position ground truth⁹ at time k . The velocity $\overline{\text{RMSE}}_k^v(N)$ is calculated in the same manner, by replacing $\hat{\mathbf{x}}_k^p(n)$ and \mathbf{x}_k^{pg} with the velocity state estimate $\hat{\mathbf{x}}_k^v(n)$ and velocity ground truth \mathbf{x}_k^{vg} respectively.

⁹The ground truth is not noisy in the example considered, it only exhibits maneuvers that have to be modeled as process noise by the tracker. It should be pointed out that white process noise is needed for the state to be a Markov process in order to estimate it recursively.

TABLE VI
Average RMSE^p (in m) for each scenario and 95% confidence region for the true RMSE^p

	U-turn scenario	S-turn scenario
OOSM-AE-Q1	217.8 [191.3, 252.7]	539.2 [473.6, 625.5]
OOSM-AE-Q2	208.1 [182.8, 241.4]	476.0 [418.1, 552.2]
OOSM-AE-Q3	182.8 [160.6, 212.1]	416.6 [365.9, 483.3]
IMMOOSM-AE	84.6 [74.3, 98.1]	188.3 [165.4, 218.4]

TABLE VII
Average RMSE^v (in m/s) for each scenario and 95% confidence region for the true RMSE^v

	U-turn scenario	S-turn scenario
OOSM-AE-Q1	30.6 [26.9, 35.5]	30.8 [27.1, 35.7]
OOSM-AE-Q2	28.7 [25.2, 33.3]	28.6 [25.1, 33.2]
OOSM-AE-Q3	26.3 [23.1, 30.5]	27.0 [23.7, 31.3]
IMMOOSM-AE	11.3 [9.9, 13.1]	11.9 [10.5, 13.8]

TABLE VIII
Track loss for the S-turn scenario

	No. of lost tracks
OOSM-AE-Q1	87
OOSM-AE-Q2	76
OOSM-AE-Q3	57
IMMOOSM-AE	1

The 95% confidence region for the true position RMSE given the average $\overline{\text{RMSE}}(N)$ is, according to Appendix C, given by the following interval.

$$\frac{\text{RMSE}}{\overline{\text{RMSE}}(N)}$$

$$\in \left[\left(\frac{1}{N} \chi_N^2(97.5\%) \right)^{-1/2}, \left(\frac{1}{N} \chi_N^2(2.5\%) \right)^{-1/2} \right] \quad (52)$$

which for $N = 100$ becomes

$$\text{RMSE} \in [0.88\overline{\text{RMSE}}(N), 1.16\overline{\text{RMSE}}(N)] \quad (53)$$

The above is used for the average over all time steps, i.e.,

$$\overline{\text{RMSE}}^p(N) = \frac{\sum_{k=1}^K \overline{\text{RMSE}}_k^p(N)}{K} \quad (54)$$

with K being the total number of time steps. The 95% confidence region for the average velocity RMSE is obtained in the same manner. These 95% confidence regions are presented in Tables VI and VII for position and velocity, respectively.

Clearly, the IMM estimation shows its value versus any single-model based filter, no matter what the latter's choice of process noise PSD.

The track is defined to be lost when the distance between the track position estimate and the ground truth becomes greater than 1500 m for more than 10 s consecutively. There are no lost tracks for the U-turn scenario for all four trackers. The number of lost tracks for the S-turn scenario are presented in Table VIII. It can

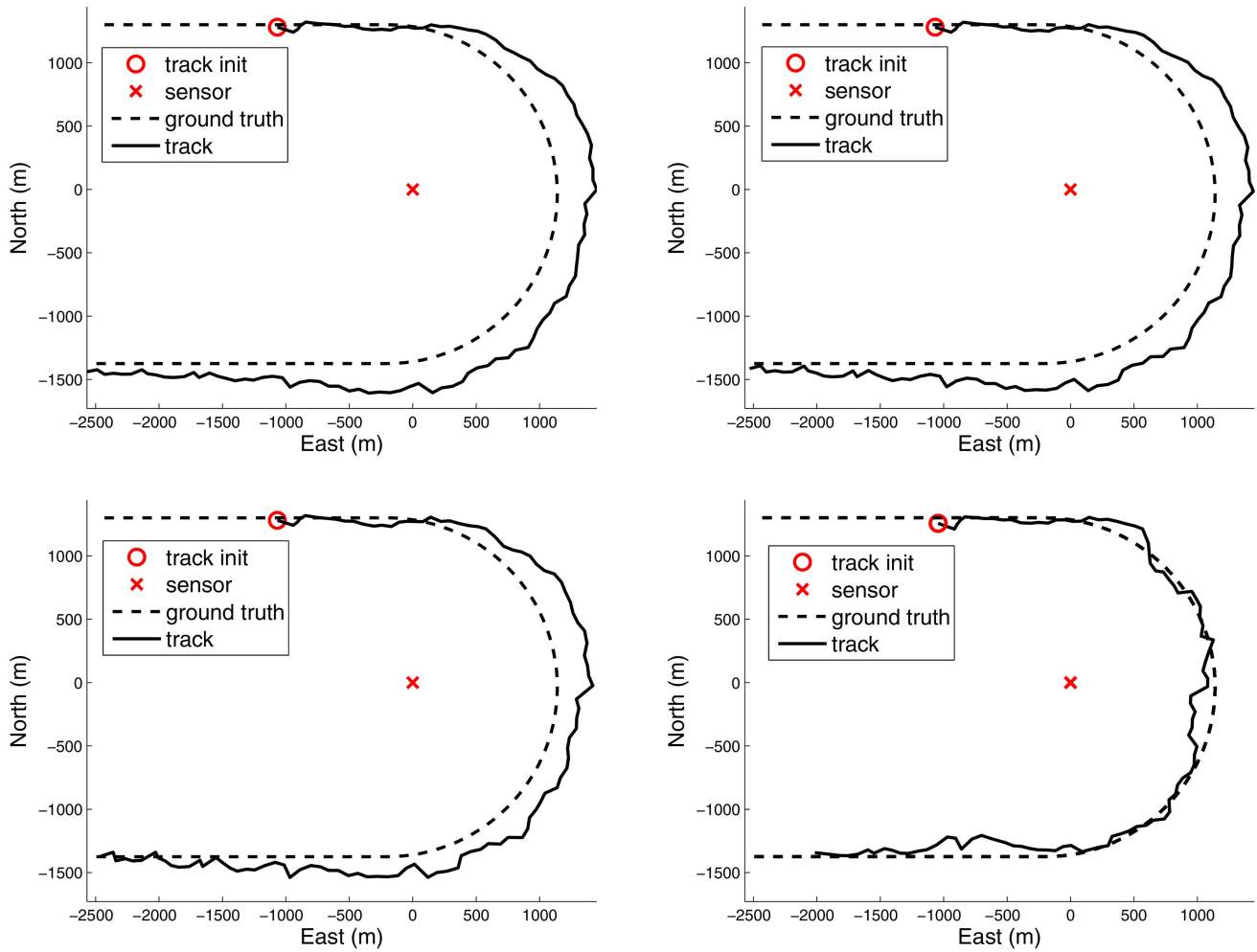


Fig. 5. OOSM-AE-Q1 (top left), OOSM-AE-Q2 (top right), OOSM-AE-Q3 (bottom left) and IMMOOSM-AE (bottom right) single run result for the U-turn scenario

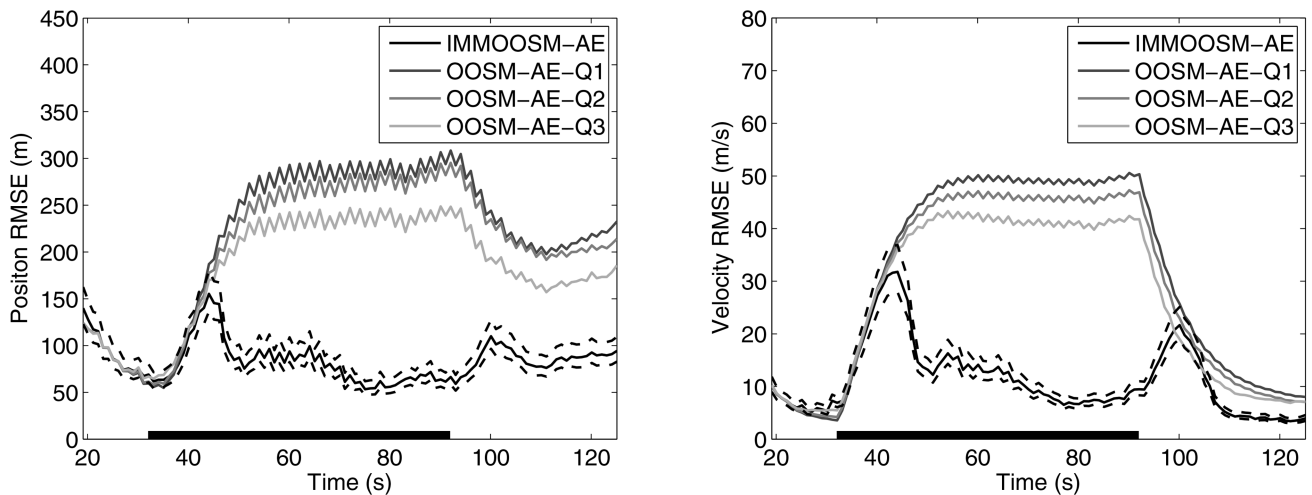


Fig. 6. Average position RMSE (left) and average velocity RMSE (right) for the U-turn scenario. The dashed lines around the IMMOOSM-AE curve represent the variability (2σ) of its performance.

be observed that the IMM filter is able to track the target without very little lost tracks, while the single-models filter suffer from significant lost tracks. The number of lost tracks is observed to be higher for the lower process noise single-model filter.

For a single run of the U-turn scenario, the estimated trajectories with OOSM-AE-Q1, OOSM-AE-Q2, OOSM-AE-Q3 and IMMOOSM-AE are shown in Fig 5. Again, no single-model filter performs even close to the IMM. It can be observed that the higher process noise

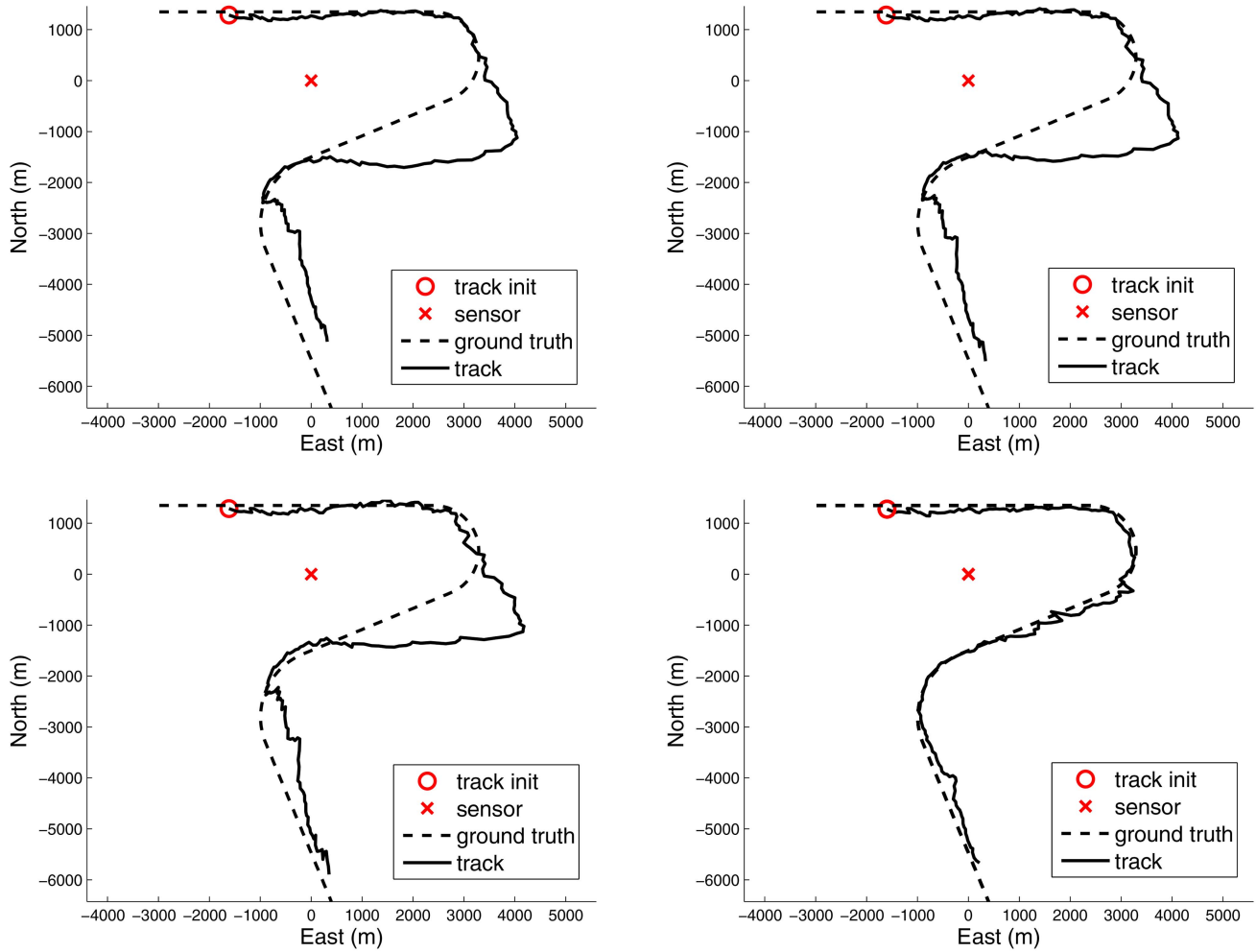


Fig. 7. OOSM-AE-Q1 (top left), OOSM-AE-Q2 (top right), OOSM-AE-Q3 (bottom left) and IMMOOSM-AE (bottom right) single run result for the S-turn scenario

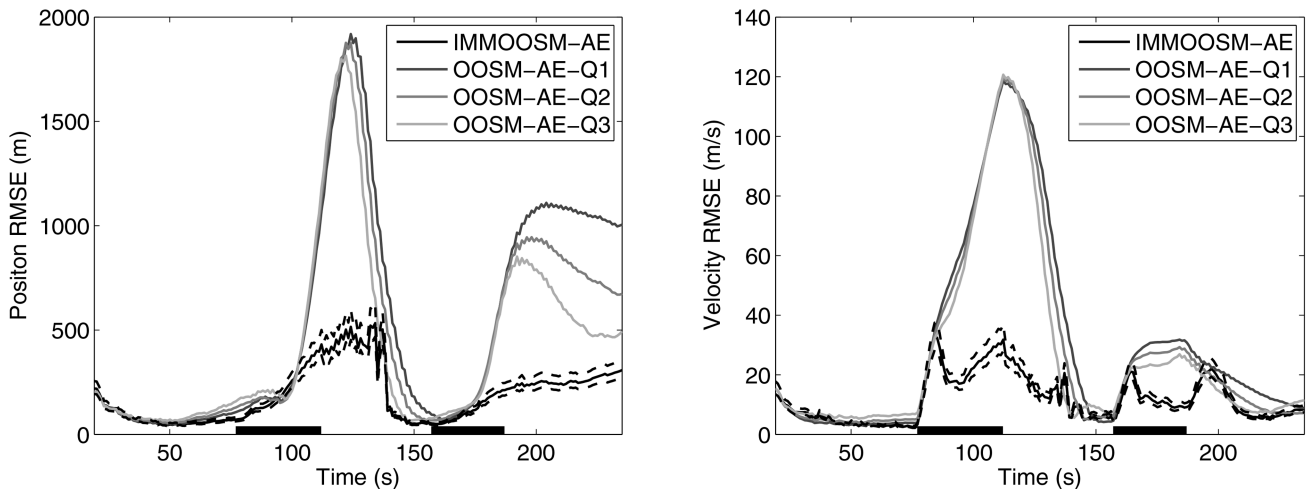


Fig. 8. Average position RMSE (left) and average velocity RMSE (right) for the S-turn scenario. The dashed lines around the IMMOOSM-AE curve represent the variability (2σ) of its performance.

single-model filter, OOSM-AE-Q3, is able to track the maneuvering target better than its lower process noise counterparts.

The position and velocity RMSE from 100 Monte Carlos runs for the U-turn scenario for OOSM-AE-Q1, OOSM-AE-Q2, OOSM-AE-Q3 and IMMOOSM-

AE are shown in Fig. 6. The dashed lines indicate the 95% confidence region for RMSE for IMMOOSM-AE. It can be seen that the variability of the performance of the IMMOOSM-AE is much smaller than the difference between it and the performance of the OOSM-AE filters. The maneuvering interval is shown as a thicker line on the time axis.

For a single run of the S-turn scenario, the estimated trajectories with OOSM-AE-Q1, OOSM-AE-Q2, OOSM-AE-Q3 and IMMOOSM-AE are shown in Fig 7. It can be observed in this particular run that none of the single-model filters are able to cope with the first sharp turn (4.5 deg/s). On the other hand, the IMM filter is able to track the maneuvering targets through both turns.

The position and velocity RMSE from 100 Monte Carlos runs for the S-turn scenario for OOSM-AE-Q1, OOSM-AE-Q2, OOSM-AE-Q3 and IMMOOSM-AE are shown in Fig. 8. The dashed lines indicate the 95% confidence region for RMSE for IMMOOSM-AE. The maneuvering intervals are shown as thicker lines on the time axis.

VI. CONCLUSIONS

The IMMOOSM-AE estimator is capable of tracking a maneuvering target by fusing the measurements from an EO (or ESM) sensor and the delayed measurements from an acoustic sensor when both are on the same stationary platform. As demonstrated in the test scenarios, the estimation accuracy in terms of RMSE is improved significantly over the single-model based OOSM-AE.

APPENDIX A GHM FOR CV

The GHM transition model, g^{CV} , for the CV model is

$$g^{CV}[\hat{\mathbf{x}}^A(t_j^{e2} | t_k^{s1}), \hat{\mathbf{x}}^E(t_k^{s1})] = [g_1^{CV}(\cdot) \quad g_2^{CV}(\cdot) \quad g_3^{CV}(\cdot) \quad g_4^{CV}(\cdot) \quad g_5^{CV}(\cdot) \quad g_6^{CV}(\cdot)]' \quad (55)$$

where

$$g_1^{CV} = x(t_j^{e2}) - x(t_k^{s1}) - \dot{x}(t_k^{s1})T_{j,k} \quad (56)$$

$$g_2^{CV} = y(t_j^{e2}) - y(t_k^{s1}) - \dot{y}(t_k^{s1})T_{j,k} \quad (57)$$

$$g_3^{CV} = \dot{x}(t_j^{e2}) - \dot{x}(t_k^{s1}) \quad (58)$$

$$g_4^{CV} = \dot{y}(t_j^{e2}) - \dot{y}(t_k^{s1}) \quad (59)$$

$$g_5^{CV} = 0 \quad (60)$$

$$g_6^{CV} = t_j^{e2} + \frac{r_{j,\ell}}{c^p} - t_k^{s2} \quad (61)$$

and

$$T_{j,k} = t_j^{e2} - t_k^{s1} < 0 \quad (62)$$

$$\begin{aligned} r_{j,\ell} &= \sqrt{[x(t_j^{e2}) - x^s(t_\ell^{s2})]^2 + [y(t_j^{e2}) - y^s(t_\ell^{s2})]^2} \\ &= \sqrt{x(t_j^{e2})^2 + y(t_j^{e2})^2} \end{aligned} \quad (63)$$

The Jacobian matrix, \mathbf{A}^{CV} , for the CV model is

$$\mathbf{A}^{CV} = \begin{bmatrix} 1 & 0 & 0 & 0 & 0 & \frac{\partial g_1^{CV}}{\partial t_j^{e2}} \\ 0 & 1 & 0 & 0 & 0 & \frac{\partial g_2^{CV}}{\partial t_j^{e2}} \\ 0 & 0 & 1 & 0 & 0 & 0 \\ 0 & 0 & 0 & 1 & 0 & 0 \\ 0 & 0 & 0 & 0 & 1 & 0 \\ \frac{\partial g_6^{CV}}{\partial x(t_j^{e2})} & \frac{\partial g_6^{CV}}{\partial y(t_j^{e2})} & 0 & 0 & 0 & 1 \end{bmatrix} \quad (64)$$

where

$$\frac{\partial g_1^{CV}}{\partial t_j^{e2}} = -\dot{x}(t_k^{s1}) \quad (65)$$

$$\frac{\partial g_2^{CV}}{\partial t_j^{e2}} = -\dot{y}(t_k^{s1}) \quad (66)$$

$$\begin{aligned} \frac{\partial g_6^{CV}}{\partial x(t_j^{e2})} &= \frac{[x(t_j^{e2} | t_k^{s1})]^p - x^s(t_\ell^{s2})}{c^p \sqrt{[x(t_j^{e2} | t_k^{s1})]^p - x^s(t_\ell^{s2})]^2 + [y(t_j^{e2} | t_k^{s1})]^p - y^s(t_\ell^{s2})]^2}} \\ &= \frac{[x(t_j^{e2} | t_k^{s1})]^p}{c^p \sqrt{[x(t_j^{e2} | t_k^{s1})]^p]^2 + [y(t_j^{e2} | t_k^{s1})]^p]^2}} \end{aligned} \quad (67)$$

$$\begin{aligned} \frac{\partial g_6^{CV}}{\partial y(t_j^{e2})} &= \frac{[y(t_j^{e2} | t_k^{s1})]^p - y^s(t_\ell^{s2})}{c^p \sqrt{[x(t_j^{e2} | t_k^{s1})]^p - x^s(t_\ell^{s2})]^2 + [y(t_j^{e2} | t_k^{s1})]^p - y^s(t_\ell^{s2})]^2}} \\ &= \frac{[y(t_j^{e2} | t_k^{s1})]^p}{c^p \sqrt{[x(t_j^{e2} | t_k^{s1})]^p]^2 + [y(t_j^{e2} | t_k^{s1})]^p]^2}} \end{aligned} \quad (68)$$

APPENDIX B GHM FOR CT

The GHM transition model, g^{CT} , for the CT model is

$$g^{CT}[\hat{\mathbf{x}}^A(t_j^{e2} | t_k^{s1}), \hat{\mathbf{x}}^E(t_k^{s1})] = [g_1^{CT}(\cdot) \quad g_2^{CT}(\cdot) \quad g_3^{CT}(\cdot) \quad g_4^{CT}(\cdot) \quad g_5^{CT}(\cdot) \quad g_6^{CT}(\cdot)]' \quad (69)$$

where

$$\begin{aligned} g_1^{CT} &= x(t_j^{e2}) - x(t_k^{s1}) - \frac{\sin[\omega(t_k^{s1})T_{j,k}]}{\omega(t_k^{s1})} \dot{x}(t_k^{s1}) \\ &\quad + \frac{1 - \cos[\omega(t_k^{s1})T_{j,k}]}{\omega(t_k^{s1})} \dot{y}(t_k^{s1}) \end{aligned} \quad (70)$$

$$\begin{aligned} g_2^{CT} &= y(t_j^{e2}) - y(t_k^{s1}) - \frac{1 - \cos[\omega(t_k^{s1})T_{j,k}]}{\omega(t_k^{s1})} \dot{x}(t_k^{s1}) \\ &\quad - \frac{\sin[\omega(t_k^{s1})T_{j,k}]}{\omega(t_k^{s1})} \dot{y}(t_k^{s1}) \end{aligned} \quad (71)$$

$$g_3^{\text{CT}} = \dot{x}(t_j^{\ell_2}) - \cos[\omega(t_k^s)T_{j,k}]\dot{x}(t_k^s) + \sin[\omega(t_k^s)T_{j,k}]\dot{y}(t_k^s) \quad (72)$$

$$g_4^{\text{CT}} = \dot{y}(t_j^{\ell_2}) - \sin[\omega(t_k^s)T_{j,k}]\dot{x}(t_k^s) - \cos[\omega(t_k^s)T_{j,k}]\dot{y}(t_k^s) \quad (73)$$

$$g_5^{\text{CT}} = \omega(t_j^{\ell_2}) - \omega(t_k^s) \quad (74)$$

$$g_6^{\text{CT}} = t_j^{\ell_2} + \frac{r_{j,\ell}}{c^p} - t_k^s \quad (75)$$

and

$$T_{j,k} = t_j^{\ell_2} - t_k^s < 0 \quad (76)$$

$$r_{j,\ell} = \sqrt{x(t_j^{\ell_2})^2 + y(t_j^{\ell_2})^2} \quad (77)$$

The Jacobian matrix, \mathbf{A}^{CT} , for the CT model is

$$\mathbf{A}^{\text{CT}} = \begin{bmatrix} 1 & 0 & 0 & 0 & 0 & \frac{\partial g_1^{\text{CT}}}{\partial t_j^{\ell_2}} \\ 0 & 1 & 0 & 0 & 0 & \frac{\partial g_2^{\text{CT}}}{\partial t_j^{\ell_2}} \\ 0 & 0 & 1 & 0 & 0 & \frac{\partial g_3^{\text{CT}}}{\partial t_j^{\ell_2}} \\ 0 & 0 & 0 & 1 & 0 & \frac{\partial g_4^{\text{CT}}}{\partial t_j^{\ell_2}} \\ 0 & 0 & 0 & 0 & 1 & 0 \\ \frac{\partial g_6^{\text{CT}}}{\partial x(t_j^{\ell_2})} & \frac{\partial g_6^{\text{CT}}}{\partial y(t_j^{\ell_2})} & 0 & 0 & 0 & 1 \end{bmatrix} \quad (78)$$

where

$$\frac{\partial g_1^{\text{CT}}}{\partial t_j^{\ell_2}} = -\dot{x}(t_k^s)\cos[\omega(t_k^s)T_{j,k}] + \dot{y}(t_k^s)\sin[\omega(t_k^s)T_{j,k}] \quad (79)$$

$$\frac{\partial g_2^{\text{CT}}}{\partial t_j^{\ell_2}} = -\dot{x}(t_k^s)\sin[\omega(t_k^s)T_{j,k}] - \dot{y}(t_k^s)\cos[\omega(t_k^s)T_{j,k}] \quad (80)$$

$$\frac{\partial g_3^{\text{CT}}}{\partial t_j^{\ell_2}} = \omega(t_k^s)\dot{x}(t_k^s)\sin[\omega(t_k^s)T_{j,k}] + \omega(t_k^s)\dot{y}(t_k^s)\cos[\omega(t_k^s)T_{j,k}] \quad (81)$$

$$\frac{\partial g_4^{\text{CT}}}{\partial t_j^{\ell_2}} = -\omega(t_k^s)\dot{x}(t_k^s)\cos[\omega(t_k^s)T_{j,k}] + \omega(t_k^s)\dot{y}(t_k^s)\sin[\omega(t_k^s)T_{j,k}] \quad (82)$$

$$\begin{aligned} & \frac{\partial g_6^{\text{CT}}}{\partial x(t_j^{\ell_2})} \\ &= \frac{[[x(t_j^{\ell_2} | t_k^s)]^p - x^s(t_k^s)]}{c^p \sqrt{[[x(t_j^{\ell_2} | t_k^s)]^p - x^s(t_k^s)]^2 + [[y(t_j^{\ell_2} | t_k^s)]^p - y^s(t_k^s)]^2}} \\ &= \frac{[x(t_j^{\ell_2} | t_k^s)]^p}{c^p \sqrt{[[x(t_j^{\ell_2} | t_k^s)]^p]^2 + [[y(t_j^{\ell_2} | t_k^s)]^p]^2}} \end{aligned} \quad (83)$$

$$\begin{aligned} & \frac{\partial g_6^{\text{CT}}}{\partial y(t_j^{\ell_2})} \\ &= \frac{[[y(t_j^{\ell_2} | t_k^s)]^p - y^s(t_k^s)]}{c^p \sqrt{[[x(t_j^{\ell_2} | t_k^s)]^p - x^s(t_k^s)]^2 + [[y(t_j^{\ell_2} | t_k^s)]^p - y^s(t_k^s)]^2}} \\ &= \frac{[y(t_j^{\ell_2} | t_k^s)]^p}{c^p \sqrt{[[x(t_j^{\ell_2} | t_k^s)]^p]^2 + [[y(t_j^{\ell_2} | t_k^s)]^p]^2}} \end{aligned} \quad (84)$$

and

$$[T_{j,k}]^p = [t_j^{\ell_2}]^p - t_k^s \quad (85)$$

APPENDIX C CONFIDENCE REGION FOR TRUE RMSE

The position or velocity error, given by $\hat{\mathbf{x}} - \mathbf{x}^g$, is assumed to follow a zero-mean Gaussian distribution with unknown variance, RMSE^2 . N independent Monte Carlo observations are taken of this error, $\hat{\mathbf{x}}(n) - \mathbf{x}^g$, $n = 1, \dots, N$. The maximum likelihood estimator, $\overline{\text{RMSE}}^2(N)$, of RMSE^2 is thus given by

$$\overline{\text{RMSE}}^2(N) = \frac{1}{N} \sum_{n=1}^N (\hat{\mathbf{x}}(n) - \mathbf{x}^g)^2 \quad (86)$$

The square $\overline{\text{RMSE}}^2(N)$ follows a scaled chi-squared distribution with N degrees of freedom, i.e. $\overline{\text{RMSE}}^2(N) \sim (\text{RMSE}^2/N)\chi_N^2$. Note that the position and velocity errors are 2-dimensional. However, the x and y errors are correlated, so the number of degrees of freedom is somewhere between N and $2N$. To be conservative, N is chosen, which will give a larger confidence region in the sequel.

The 95% probability interval for the ratio $\overline{\text{RMSE}}^2(N)/\text{RMSE}^2$ for $N = 100$ is given below.

$$\begin{aligned} \frac{\overline{\text{RMSE}}^2(N)}{\text{RMSE}^2} &\in \left[\left(\frac{1}{100} \right) \chi_N^2(2.5\%), \left(\frac{1}{100} \right) \chi_N^2(97.5\%) \right] \\ &= [0.74, 1.3] \end{aligned} \quad (87)$$

The 95% confidence region for RMSE^2 given $\overline{\text{RMSE}}^2(N)$ is thus

$$\frac{\text{RMSE}^2}{\overline{\text{RMSE}}^2(N)} \in [(0.74)^{-1}, (1.3)^{-1}] = [0.77, 1.35] \quad (88)$$

Therefore, the 95% confidence region for RMSE given $\overline{\text{RMSE}}(N)$ is

$$\frac{\text{RMSE}}{\overline{\text{RMSE}}(N)} \in [\sqrt{0.77}, \sqrt{1.35}] = [0.88, 1.16] \quad (89)$$

i.e.,

$$\text{RMSE} \in [0.88\overline{\text{RMSE}}(N), 1.16\overline{\text{RMSE}}(N)] \quad (90)$$

REFERENCES

- [1] V. Aidala
 “Kalman filter behavior in bearings-only tracking applications,”
Aerospace and Electronic Systems, IEEE Transactions on, vol. AES-15, no. 1, pp. 29–39, Jan 1979.
- [2] Y. Bar-Shalom
 “Update with out-of-sequence measurements in tracking: exact solution,”
Aerospace and Electronic Systems, IEEE Transactions on, vol. 38, no. 3, pp. 769–777, Jul 2002.
- [3] Y. Bar-Shalom, M. Mallick, H. Chen, and R. Washburn
 “One-step solution for the general out-of-sequence-measurement problem in tracking,”
 in *Aerospace Conference Proceedings, 2002. IEEE*, vol. 4, 2002, pp. 4-1551–4-1559 vol.4.
- [4] Y. Bar-Shalom, X. R. Li, and T. Kirubarajan
Estimation with Applications to Tracking and Navigation: Theory, Algorithms and Software.
 John Wiley & Sons, 2001.
- [5] Y. Bar-Shalom, P. K. Willett, and X. Tian
Tracking and Data Fusion: A Handbook of Algorithms.
 YBS Publishing, 2011.
- [6] H. Blom and Y. Bar-Shalom
 “The interacting multiple model algorithm for systems with markovian switching coefficients,”
Automatic Control, IEEE Transactions on, vol. 33, no. 8, pp. 780–783, Aug 1988.
- [7] J. E. L. Cadre and C. Jauffret
 “Discrete-time observability and estimability analysis for bearings-only target motion analysis,”
IEEE Transactions on Aerospace and Electronic Systems, vol. 33, no. 1, pp. 178–201, Jan 1997.
- [8] E. Fogel and M. Gavish
 “Nth-order dynamics target observability from angle measurements,”
Aerospace and Electronic Systems, IEEE Transactions on, vol. 24, no. 3, pp. 305–308, May 1988.
- [9] C. Jauffret, D. Pillon, and A.-C. Perez-Pignol
 “Bearings-only TMA without observer maneuver,”
 in *Information Fusion, Proc. 11th International Conference on*, June 2008.
- [10] S. J. Julier and J. K. Uhlmann
 “New extension of the Kalman filter to nonlinear systems,”
 in *Proc. SPIE, Conf. Signal Processing, Sensor Fusion, and Target Recognition VI*, vol. 3068, Orlando, FL, April 1997.
- [11] A. G. Lindgren and K. F. Gong
 “Position and velocity estimation via bearing observations,”
Aerospace and Electronic Systems, IEEE Transactions on, no. 4, pp. 564–577, 1978.
- [12] E. Mazor, A. Averbuch, Y. Bar-Shalom, and J. Dayan
 “Interacting multiple model methods in target tracking: a survey,”
Aerospace and Electronic Systems, IEEE Transactions on, vol. 34, no. 1, pp. 103–123, Jan. 1998. [Online]. Available: <http://dx.doi.org/10.1109/7.640267>.
- [13] U. Orguner and F. Gustafsson
 “Target tracking using delayed measurements with implicit constraints,”
 in *Information Fusion, Proc. 11th International Conference on*, June 2008.
- [14] ———
 “Particle filtering with propagation delayed measurements,”
 in *Proc. Aerospace Conference, 2010 IEEE*, Big Sky, MT, March 2010.
- [15] A. Papoulis and S. Pillai
Probability, Random Variables, and Stochastic Processes, ser. McGraw-Hill series in electrical and computer engineering. McGraw-Hill, 2002. [Online]. Available: <https://books.google.com.sg/books?id=WM69jwEACAAJ>.
- [16] A. Petersen and R. Koch
 “Statistical analysis of Kalman filters by conversion to Gauss-Helmert models with applications to process noise estimation,”
 in *Proc. Pattern Recognition (ICPR), 2010 20th International Conference on*, Aug 2010, pp. 2386–2389.
- [17] R. Yang, Y. Bar-Shalom, and G. W. Ng
 “Bearings-only tracking with fusion from heterogenous passive sensors: ESM/EO and acoustic,”
 in *Proc. 18th Intn’l Conf. on Information Fusion*, Washington, DC, July 2015.
- [18] R. Yang, Y. Bar-Shalom, H. A. J. Huang, and G. W. Ng
 “UGHF for acoustic tracking with state-dependent propagation delay,”
 vol. 51, no. 3, July 2015, pp. 1747–1761.
- [19] R. Yang, J. Huang, G. W. Ng, and Y. Bar-Shalom
 “Interacting multiple model unscented Gauss-Helmert filter for bearings-only tracking with state-dependent propagation delay,”
 in *Information Fusion (FUSION), Proc. 17th International Conference on*, July 2014.
- [20] T. Yuan, Y. Bar-Shalom, P. Willett, E. Mozeson, S. Pollak, and D. Hardiman
 “A multiple IMM estimation approach with unbiased mixing for thrusting projectiles,”
Aerospace and Electronic Systems, IEEE Transactions on, vol. 48, no. 4, pp. 3250–3267, October 2012.



Hong An Jack Huang was born in Singapore in 1983. He received a B.E. degree from National University of Singapore (NUS) in 2008. He is currently a senior member of technical staff at DSO National Laboratories, Singapore. His research interests in target tracking include GMTI tracking, passive tracking, and image tracking.

Yaakov Bar-Shalom was born on May 11, 1941. He received the B.S. and M.S. degrees from the Technion, Israel Institute of Technology, in 1963 and 1967 and the Ph.D. degree from Princeton University in 1970, all in electrical engineering. From 1970 to 1976 he was with Systems Control, Inc., Palo Alto, California. Currently he is Board of Trustees Distinguished Professor in the Dept. of Electrical and Computer Engineering and Marianne E. Klewin Professor in Engineering at the University of Connecticut. He is also Director of the ESP (Estimation and Signal Processing) Lab. His current research interests are in estimation theory, target tracking and data fusion. He has published over 500 papers and book chapters in these areas and in stochastic adaptive control. He coauthored the monograph *Tracking and Data Association* (Academic Press, 1988), the graduate texts *Estimation and Tracking: Principles, Techniques and Software* (Artech House, 1993; translated into Russian, MGTU Bauman, Moscow, Russia, 2011), *Estimation with Applications to Tracking and Navigation: Algorithms and Software for Information Extraction* (Wiley, 2001), the advanced graduate texts *Multitarget-Multisensor Tracking: Principles and Techniques* (YBS Publishing, 1995), *Tracking and Data Fusion* (YBS Publishing, 2011), and edited the books *Multitarget-Multisensor Tracking: Applications and Advances* (Artech House, Vol. I, 1990; Vol. II, 1992; Vol. III, 2000). He has been elected Fellow of IEEE for “contributions to the theory of stochastic systems and of multi-target tracking.” He has been consulting to numerous companies and government agencies, and originated the series of Multitarget-Multisensor Tracking short courses offered via UCLA Extension, at Government Laboratories, private companies and overseas. During 1976 and 1977 he served as Associate Editor of the IEEE Transactions on Automatic Control and from 1978 to 1981 as Associate Editor of Automatica. He was Program Chairman of the 1982 American Control Conference, General Chairman of the 1985 ACC, and Co-Chairman of the 1989 IEEE International Conference on Control and Applications. During 1983–87 he served as Chairman of the Conference Activities Board of the IEEE Control Systems Society and during 1987–89 was a member of the Board of Governors of the IEEE CSS. He was a member of the Board of Directors of the International Society of Information Fusion (1999–2004) and served as General Chairman of FUSION 2000, President of ISIF in 2000 and 2002 and Vice President for Publications in 2004–13. In 1987 he received the IEEE CSS Distinguished Member Award. Since 1995 he is a Distinguished Lecturer of the IEEE AESS and has given numerous keynote addresses at major national and international conferences. He is co-recipient of the M. Barry Carlton Award for the best paper in the IEEE Transactions on Aerospace and Electronic Systems in 1995 and 2000 and recipient of the 1998 University of Connecticut AAUP Excellence Award for Research. In 2002 he received the J. Mignona Data Fusion Award from the DoD JDL Data Fusion Group. He is a member of the Connecticut Academy of Science and Engineering. In 2008 he was awarded the IEEE Dennis J. Picard Medal for Radar Technologies and Applications, and in 2012 the Connecticut Medal of Technology. In 2015, he received from the International Society for Information Fusion the Lifetime of Excellence in Information Fusion award. Since 2016, this award has been renamed as the Yaakov Bar-Shalom Award for Lifetime of Excellence in Information Fusion. He has been listed by academic.research.microsoft (top authors in engineering) as #1 among the researchers in Aerospace Engineering based on the citations of his work.





Rong Yang received her B.E. degree in information and control from Xi'an Jiao Tong University, China in 1986, M.Sc. degree in electrical engineering from the National University of Singapore in 2000, and Ph.D. degree in electrical engineering from Nanyang Technological University, Singapore in 2012. She is currently a Principal Member of Technical Staff at DSO National Laboratories, Singapore. Her research interests include passive tracking, low observable target tracking, GMTI tracking, hybrid dynamic estimation and data fusion. She received the FUSION 2014 Best Paper Award (First runner up).



Gee Wah Ng received his M.Sc. and Ph.D. from University of Manchester Institute of Science and Technology, United Kingdom. He is currently a Distinguished Member of Technical Staff and Programme Director (Information Exploitation) of Information Division at DSO National Laboratories. He has delivered many projects in the decision support areas and has authored three books. He is active in international conferences in the areas of information fusion and intelligent systems. His research interests in data and information fusion include target tracking, computational intelligence, machine learning, self-tuning and sensor networks.